Science and Engineering Research Council
Rutherford Appleton Laboratory
CHILTON, DIDCOT, OXON, OX11 0QX

RAL-87-056

Temperature Imaging Using Epithermal Neutrons

P H Fowler and A D Taylor

August 1987

RAL-87-056

TEMPERATURE IMAGING USING EPITHERMAL NEUTRONS

P H Fowler

H H Wills Physics Laboratory
University of Bristol
Bristol, BS8 1TL

and

A D Taylor

Rutherford Appleton Laboratory
Chilton, Didcot, Oxon, OX11 0QX, UK

Presented at the Neutron Resonance Radiography Workshop
Los Alamos National Laboratory, Los Alamos NM, USA
July 27-29, 1987

DEMONSTRATION OF TEMPERATURE IMAGING USING EPITHERMAL NEUTRONS

INTRODUCTION

Three years ago in spring 1984 one of us (PHF) conceived the idea of attempting to measure the temperature of suitable targets both remotely and non-invasively using epithermal neutrons. The idea was spawned following discussions with Rolls Royce in Bristol, which took place in the climate that universities and other research groups should make every effort to interact positively with industry. Neutron scientists at the Rutherford Appleton Laboratory quickly became involved, and after a period of thought and calculation, it was clear to us that the most promising resonances lay in the energy band $1 \leq E \leq 100$ eV - and that a practical demonstration was necessary.

In July 1984 it was agreed at a joint meeting with Rolls Royce at the Rutherford Appleton Laboratory that a simple and direct measurement be made to determine the feasibility of the method. Over the next few weeks a fully instrumented oven was prepared at RAL, and necessary counting, data handling and computing equipment were provided by Dr P A Seeger of the Physics Division, Los Alamos. Los Alamos was chosen as the site for the experiments as there was no suitable pulsed neutron beam of epithermal neutrons in the UK at that time.

In the third week of September the oven was set up in the beam. The arrangement of the beam line is as sketched in Figure 1. Critical to the performance of this system for our measurement are a number of features :

1 The distance between the detector and source - which was determined to be 31.85m from timing measurements of resonances in the spectra obtained. The specimen and oven were in this case mounted half way along the neutron flight path, but a better general arrangement would have the specimen close to the detector.

2 The time resolution and efficiency of the He^3 detector - which were < 1 μs and ~ 15% at 1 eV respectively.

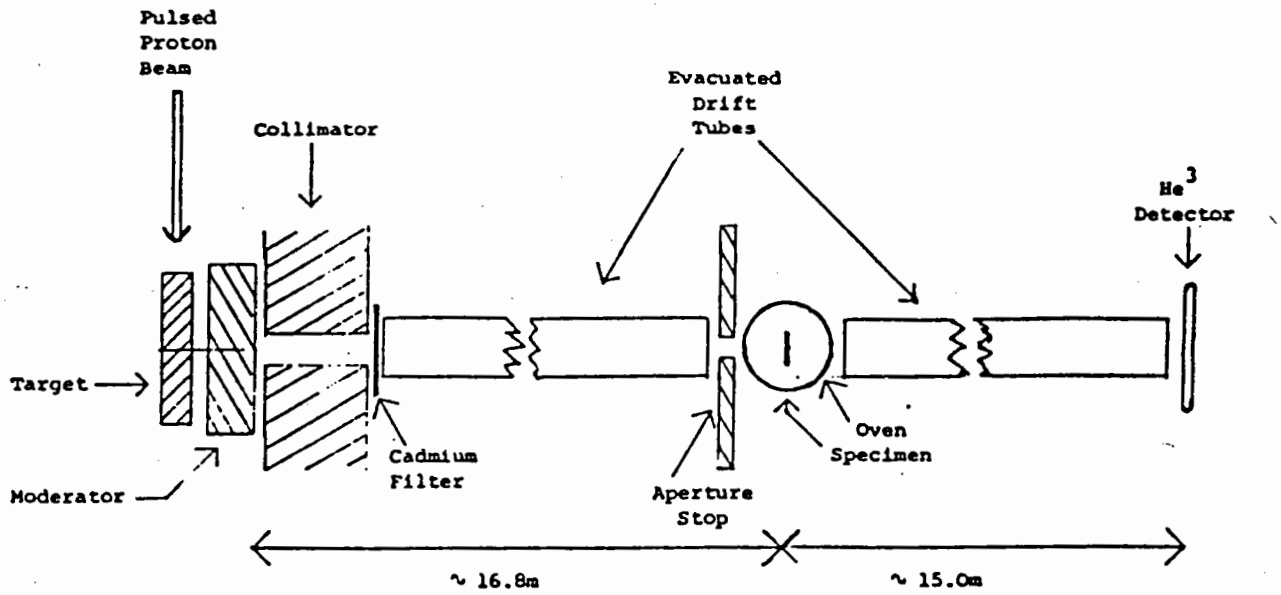

Fig. 1 Sketch of the experimental arrangement used at Los Alamos

3 The performance of the oven for holding the chosen temperature and recording the changes.

4 The stability of the whole system - so that the whole of the variation between exposures should be due to the changes made by us to the specimen in the oven.

Our main runs took place in the week beginning 24 September 1984 when we were allocated a large fraction of the running time on this beamline which totalled ~ 120 hours of useful beam. The allocation ceased by 0800 on 30 September when the machine was turned off for modifications designed to improve substantially the intensity and timing of the pulsed neutron beam. A number of runs were made at several temperatures with two tantalum foils of different thickness (27 and 106 μm) and a specimen of 8 mm thickness made from a Rolls Royce high temperature nickel based alloy Marm 002, that contains W, Ta and Hf.

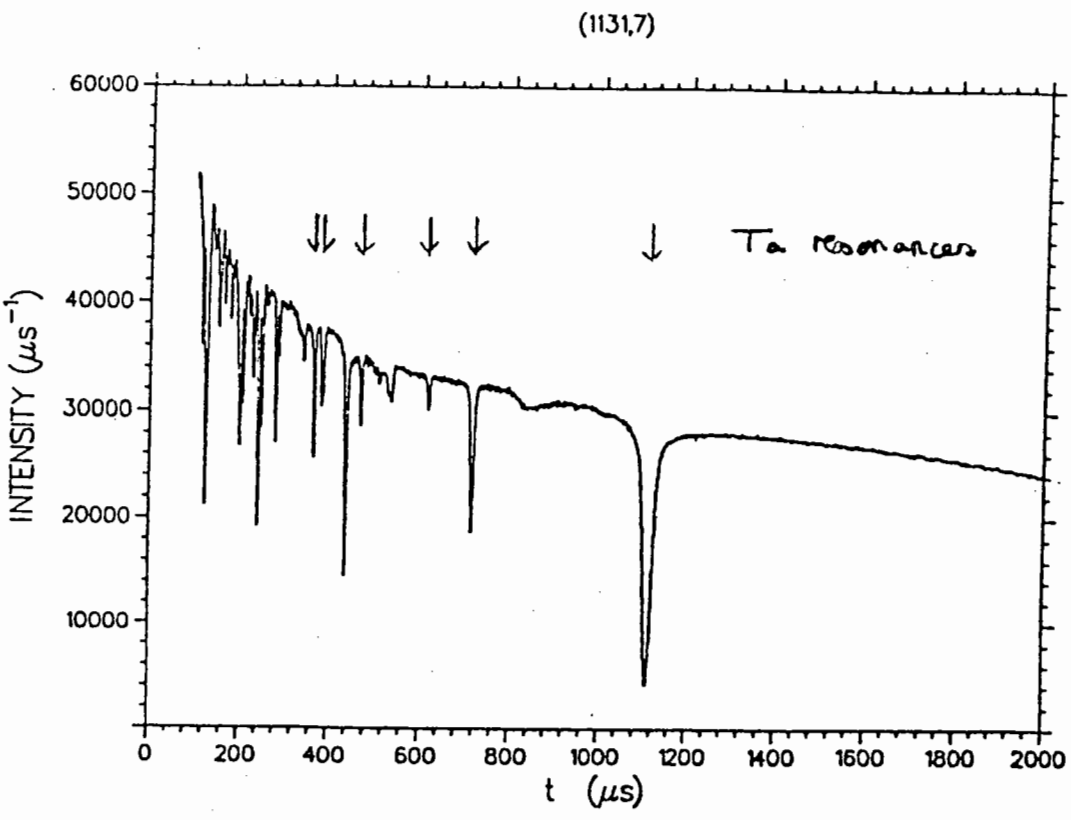

INTENSITY VERSUS DRIFT TIME

Fig. 2a The time of flight spectrum using a thin (27μm) Tantalum foil

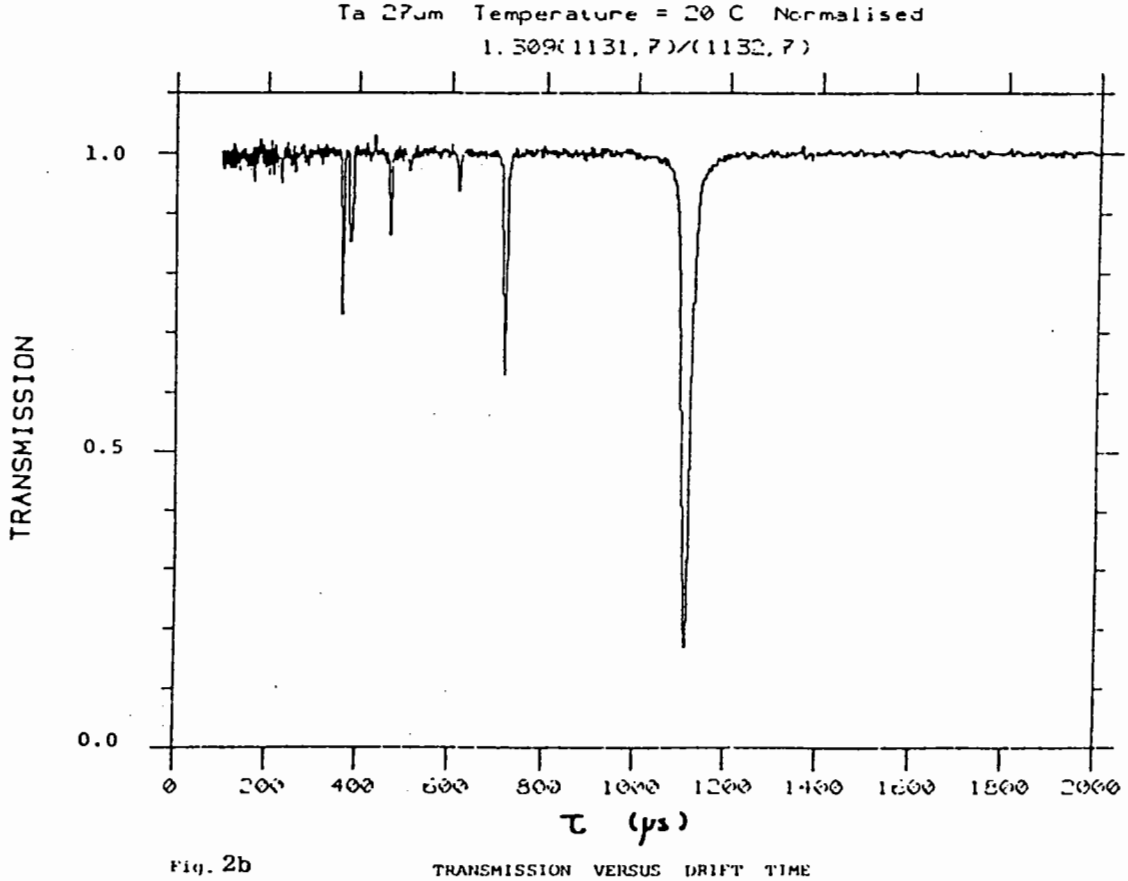

Fig. 2b TRANSMISSION VERSUS DRIFT TIME

THE RESULTS OF THE MEASUREMENTS

As an introduction to the presentation of the results we obtained [1], Figure 2a shows a typical spectrum taken with a thin tantalum foil at room temperature. The number of neutrons detected per microsecond of neutron transit time is plotted against the transit time. With a beam line of length equal to 31.85m the relation between the neutron energy E, and the indicated transit time τ, is given by

$$\tau = \frac{2300.1}{\sqrt{E}} - 1.1 \ \mu s, \qquad (1)$$

where E is measured in electron-volts. The offset of 1.1 μs due to electronic delays in the system was empirically determined. The prominent resonance centred at 1111 μs corresponds to 4.28 eV and is the well known tantalum resonance. Other tantalum resonances are indicated. There are also a number of other features in this spectrum which are due to materials in the beam unassociated with the specimen. Many of the jumble of resonances with $\tau < 300$ μs are so caused. Among the strongest background features in evidence are three deep resonance at 120 μs due to Mn^{55}, 205 μs due to Co^{59}, 440 μs due to Cd^{113} and several other features due to cadmium. The Co and Mn are present in the stainless steel from the oven walls. The cadmium features are due to the deliberate employment of a cadmium filter to remove thermal neutrons from our beam which would arrive so late that they would be associated with the wrong pulse. Such a problem is akin to higher order spectra in diffraction. In Figure 2b we show the effect of comparing two exposures, one with and one without the tantalum foil and so plotting its transmission efficiency versus transit time. Six tantalum resonances show clearly, and the complex of background lines are suppressed - the transmission is close to unity away from the Ta resonances apart from fluctuations which are at a level $\sim \pm 0.5\%$ for $\tau \geq 300$ μs. The above procedures are standard in neutron time of flight experiments.

The effect of temperature upon neutron transmission comes about due to thermal motion of the target atom which produces Doppler broadening. Due to the random nature of thermal motion of the atoms the collision energy between a monoenergetic neutron beam and the nucleus is no longer just a function of the neutron speed or energy, but is spread by an RMS quantity Δ given overleaf.

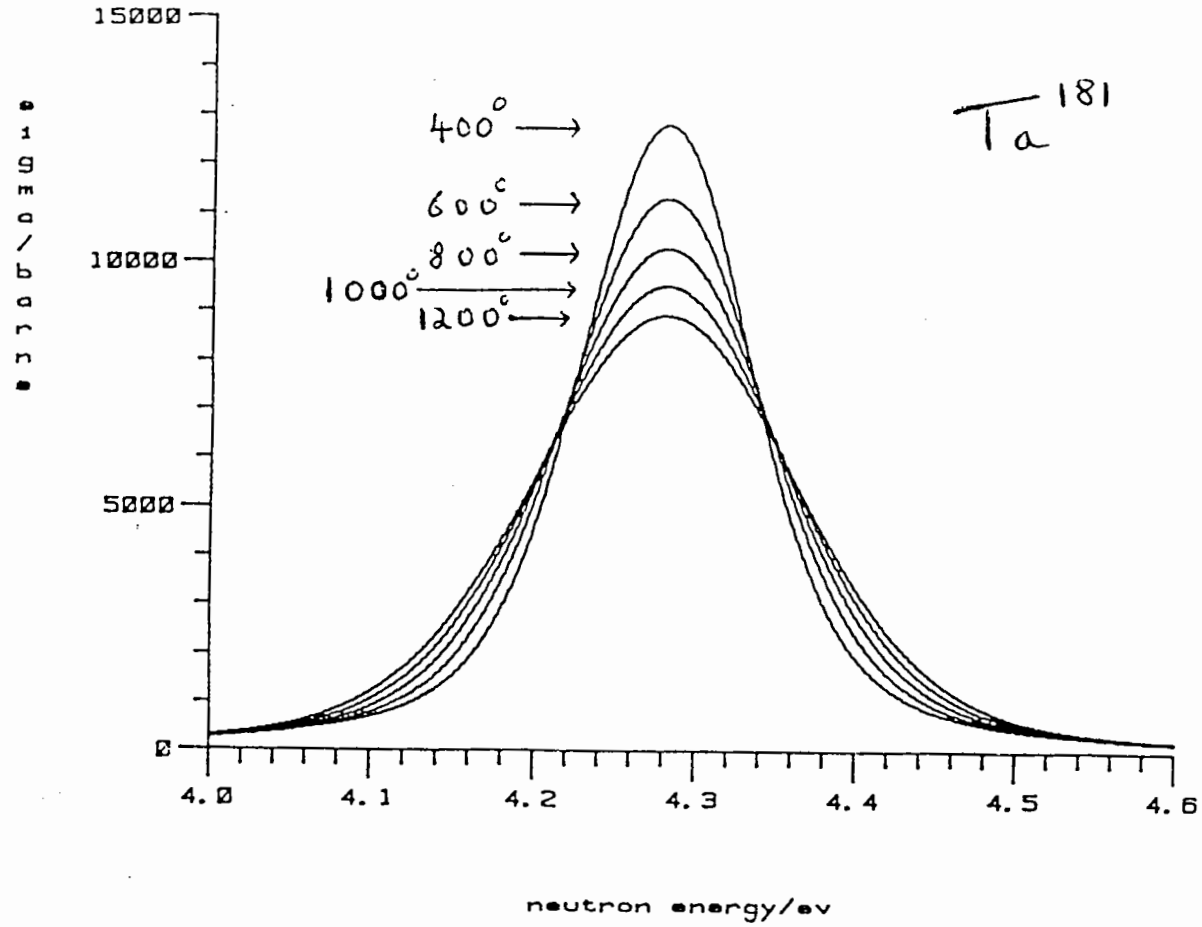

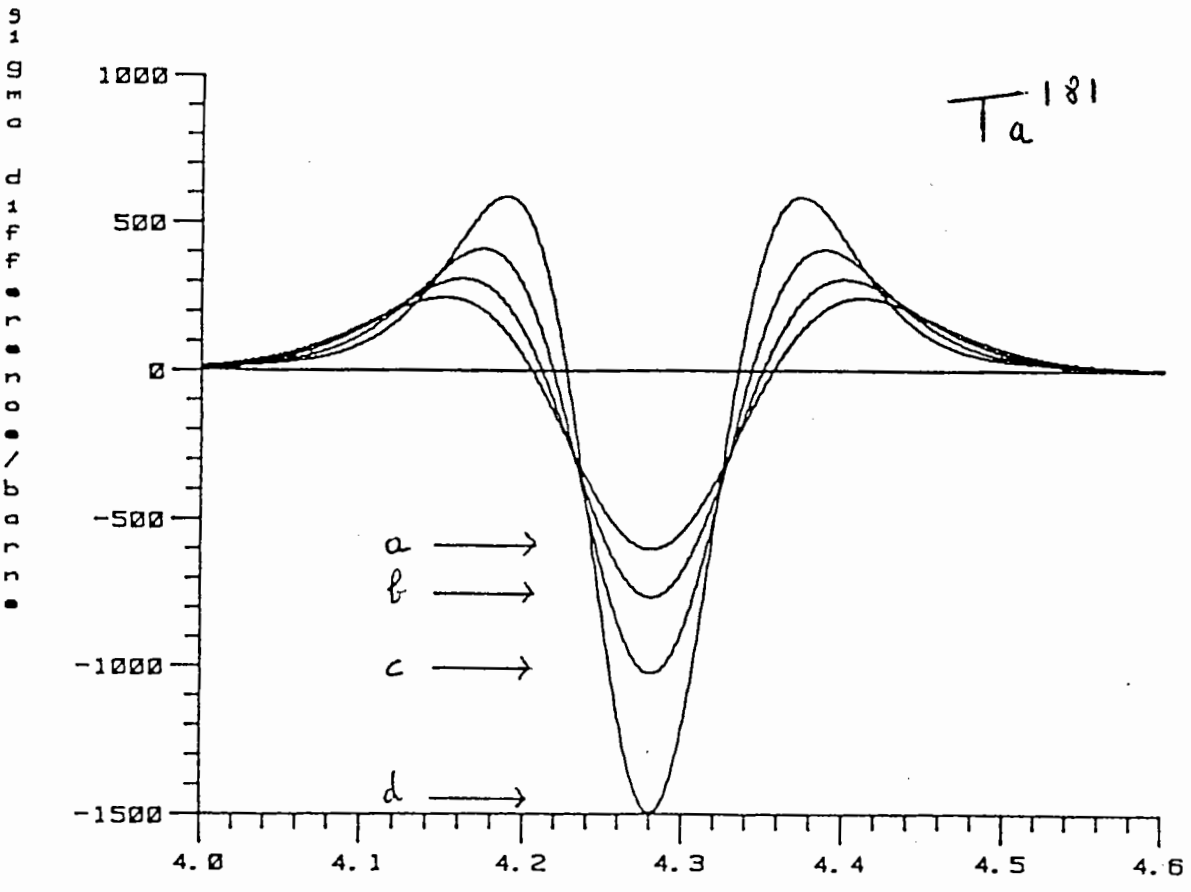

Fig. 3a,b Computed cross sections at 5 temperatures for the 4,28 eV Tantalum resonance, and the change in cross section for successive 200°K temperature increases.

$$\Delta \simeq Mu\,[v \cos\theta]_{RMS} \simeq 13.1 \frac{A}{A+1}\left[\frac{E_n T^*}{A}\right]^{\frac{1}{2}} \text{ eV}, \qquad (2)$$

where u and v are the speeds of the neutron and target atom,
M is the target atom mass and A its mass in amu,
E_n is the neutron energy in eV and T^* is the effective target temperature in °K.

T^* differs from the true temperature T due to zero point motion of the atoms, which for an element is characterised by the Debye temperature θ_c. T^* is given by the relation :

$$T^* = \frac{3\theta_c}{8} \coth\left[\frac{3\theta_c}{8T}\right]$$

At low temperatures T^* tends to θ_c, while at higher temperatures ($T \sim \theta_c$) T^* is given approximately by the relation:

$$T^* \simeq T + \frac{3\theta_c^2}{64T}$$

For alloys, especially the minority constituents, the effective value of θ_c is not clear, but it can always be determined where necessary by direct measurement of a neutron resonance at low temperature. At high temperatures, of principal concern in this paper, T can be substituted for T^* with negligible loss of accuracy.

The value of Δ thus depends upon neutron energy, temperature and atomic mass of the material. The effect of the blurring so produced is clearly ;largest around a sharp resonance where there are rapid changes of cross section and therefore transmission with neutron energy. Figures 3a and b display the results of the effective cross section (after blurring) for scattering plus absorption for the tantalum resonance at 4.28 eV showing how the broadening develops. The response of a given resonance is essentially a function of the ratio Δ/Γ where Δ is given above and Γ (the full width half maximum) is a property of the individual resonance. When Δ/Γ is low, i.e. at a very low temperature or for a very broad resonance, the blurring makes little impact, so there is a very low value for temperature sensitivity. This is the case for the intense resonances of W^{186}, Co^{59} and Mn^{55} at 18.84, 132 and 337 eV

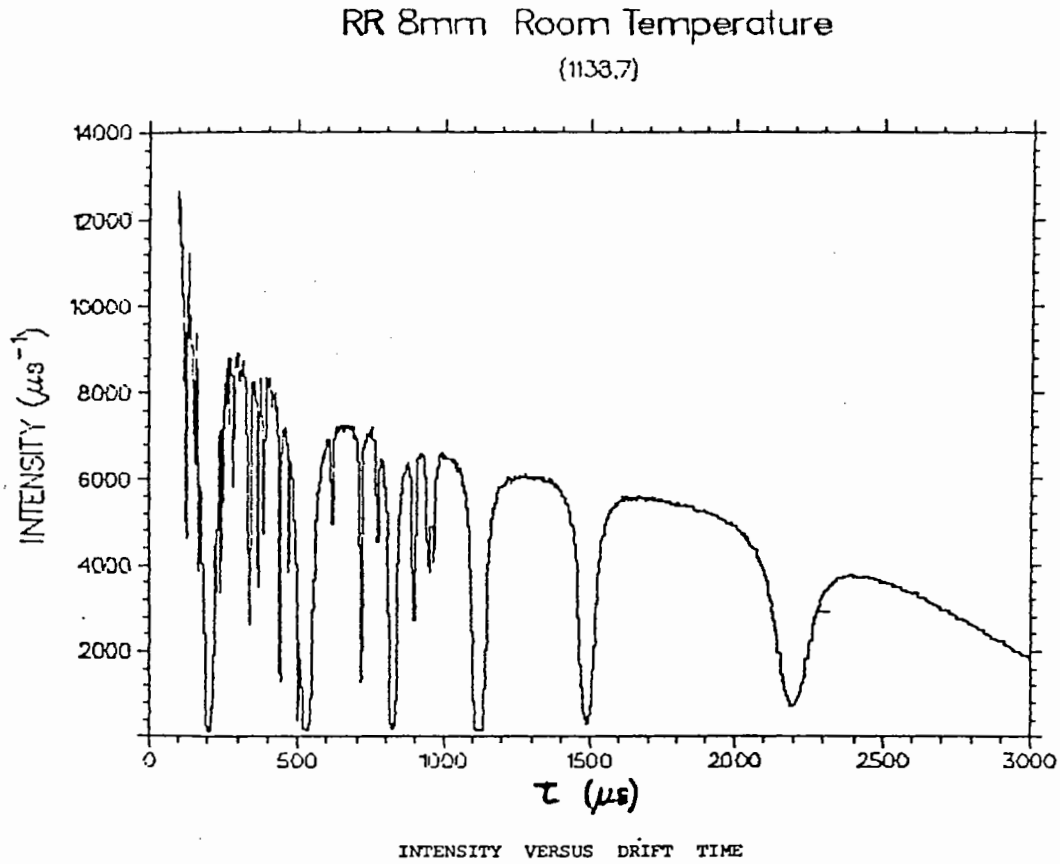

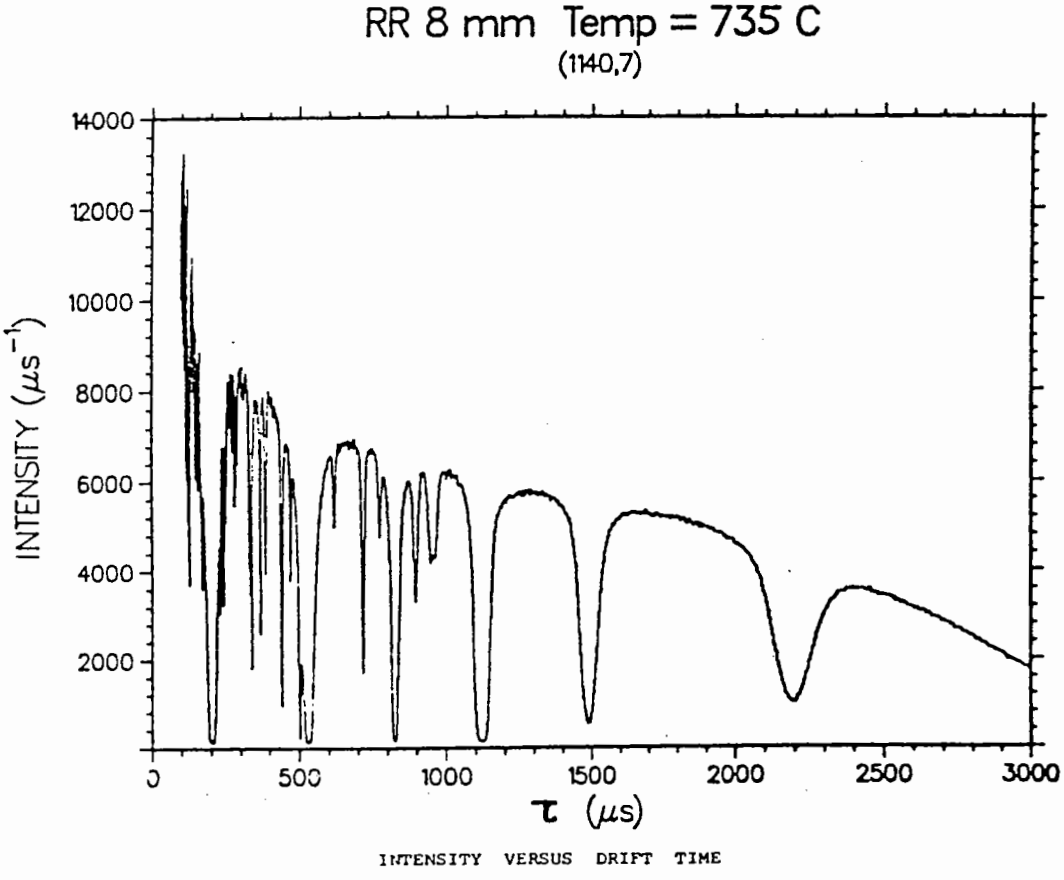

Fig. 4a,b Time of flight spectra at 20°C and 735°C using 8 mm of MARM 002

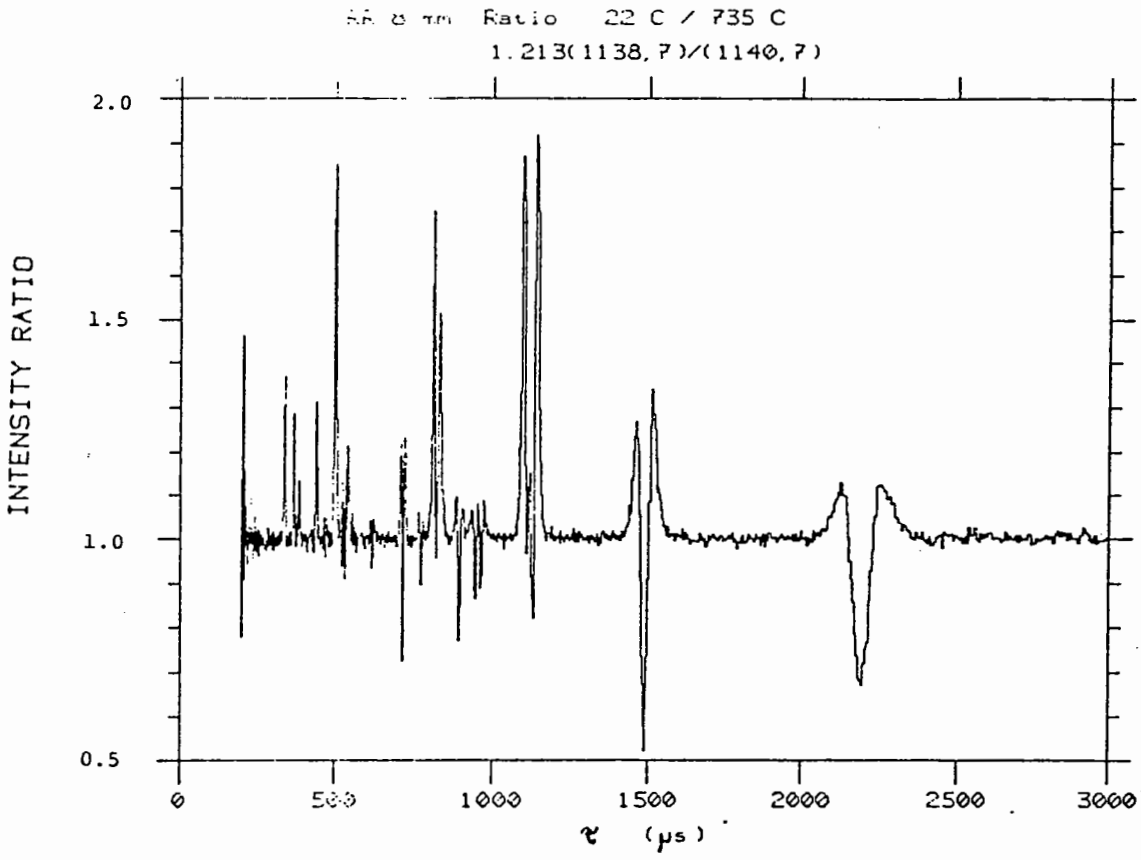

Fig. 5 The intensity versus time of flight from the data given in Figs. 4a and b.

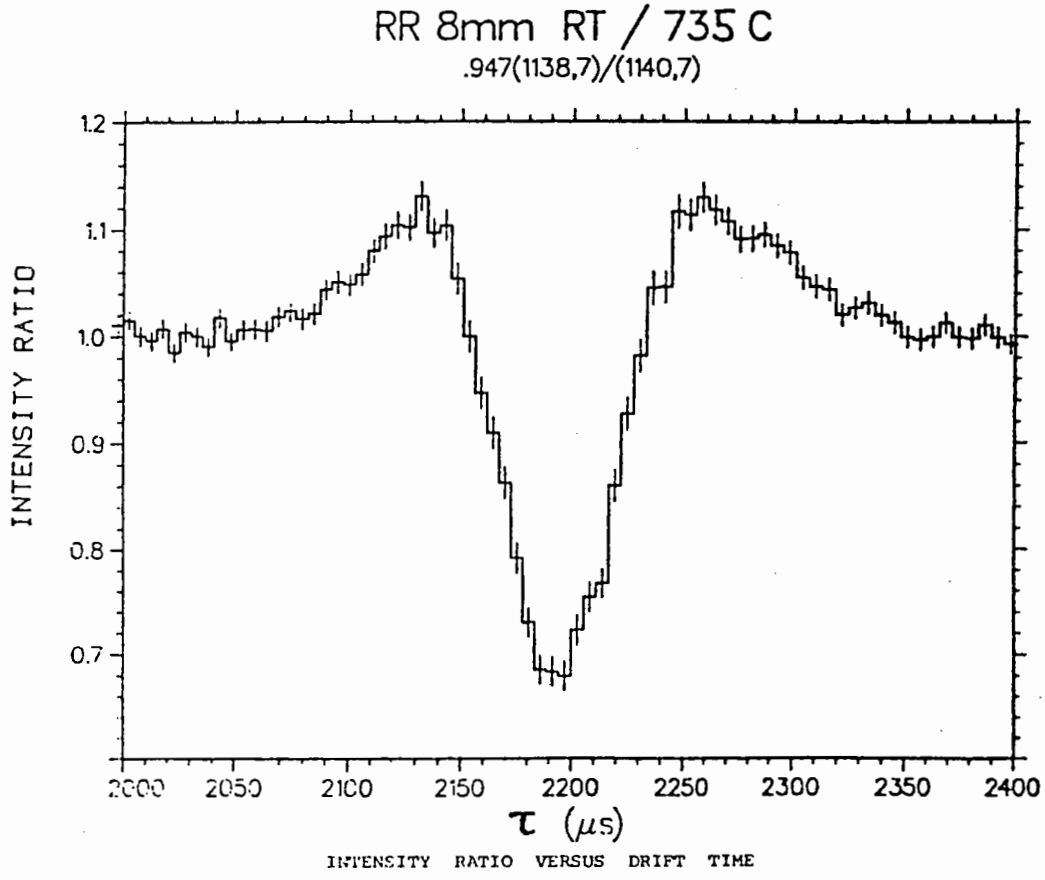

Fig. 6a Details of the intensity ratio from Fig. 5 above for the resonance at ∿ 2200 μsec due to Hf^{177}. Statistical errors are given for each bin.

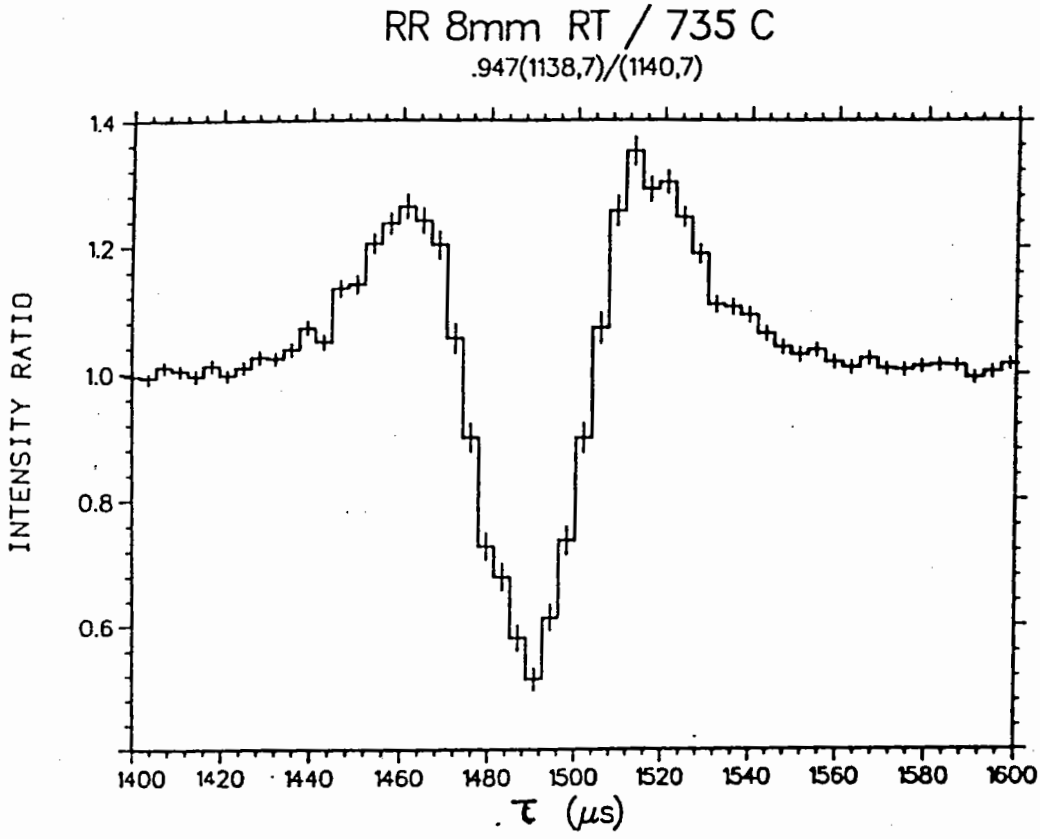

Fig. 3b INTENSITY RATIO VERSUS DRIFT TIME

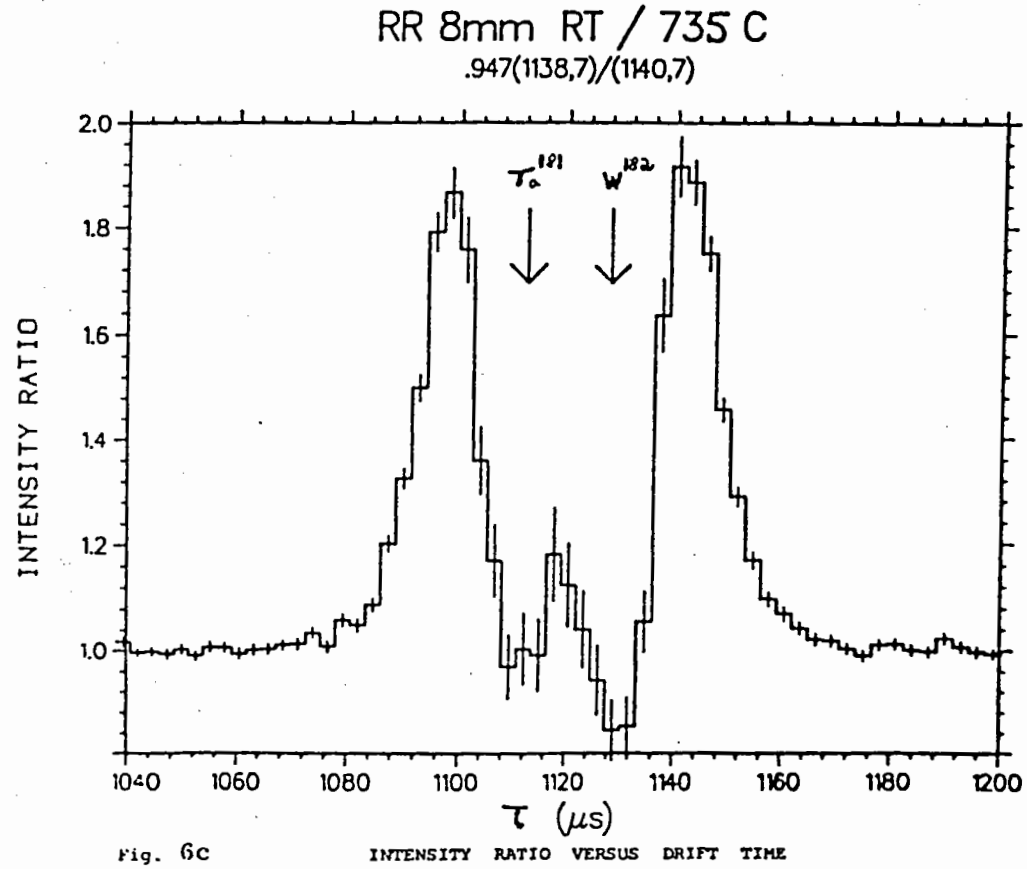

Fig. 6c INTENSITY RATIO VERSUS DRIFT TIME

respectively. Also plotted in Figure 3b is the difference in the cross section, for the pairs of temperature indicated, for the 4.28 eV Ta resonance; this displays a 'crater-like' shape for the energy response with an amplitude that as expected in fact decreases with increasing temperature, but also broadens.

The raw spectra from the runs for the extreme temperatures used (22° and 735°C) with 8 mm Rolls Royce material are shown in Figures 4a and b. Direct comparison with Figure 2a shows at once that a lot more deep resonances are present. These are due to the hafnium and tungsten that are present in addition to the tantalum. The raw measurements presented in Figure 4b differ from that in Figure 4a only in that the temperature of the specimen was held at 735°, rather than at room temperature. Casual comparison of these two figures shows small differences only, however, the differences can be vividly revealed by dividing the detected number of neutrons in each microsecond in the first neutron accumulation by those in the second. Clearly, if nothing had changed the result would be unity in all time bins (assuming the correct normalisation), but what we see in each time interval is shown in Figure 5.

Each resonance is replaced by a crater-like shape which approximates in fact to the second derivative of the resonance curve. This operation also removes the background features due to Cd etc - but not those of Mn and Co as the temperature of oven walls also changed. Figures 6a-c show these data on enlarged scales to display the principle resonances in detail. The statistical errors for each bin are shown. The effect of temperature is dramatic - with changes approaching a factor of two in neutron attenuation due just to the temperature change. In a single bin at ~ 1150 μs (width ~ 3 μs) from Figure 6c for the combined 4 eV resonances of Ta and W, the ratio is 1.77 ± 0.023 - which indicates an uncertainty of a temperature estimate of ± 25°C using this bin alone. The whole resonance in Figure 6c yields an uncertainty of the order of ± 8°C. While this resonance contains more information on temperature than any of the other resonances, the sum total of information from all the other resonances is approximately twice that of the 4 eV resonance, so that our estimate of the uncertainty in temperature estimate that could be made from the whole data set is of the order of 4.6°C. The six most informative resonances are tabulated below, two pairs overlap and each yield one estimate.

TABLE I

E_o eV	Nuclide	Flight Time μ sec	μ_o Attenuation lengths	ΔT °K Exp
1.10	Hf^{177}	2914	2.4	11.1
2.38	Hf^{177}	1489	4.9	10.4
4.16	W^{182}	1127	11.2	8.3 overlapping
4.28	Ta^{181}	1111	14.6	
7.65	W^{183}	831	2.2	14.2 overlapping
7.78	Hf^{178}	824	16.0	

μ_o is the number of attenuation lengths that the specimen presented at the centre of the resonance in the absence of any Doppler broadening.
ΔT is estimated from the experimental data.

The results above have been illustrated with analysis of measurements made using the most widely spaced pair of temperatures - so that the effects of temperature were immediately apparent. One is of course concerned as to the manner in which sensitivity to temperature differences might vary with temperature. Figure 7 shows the ratio of neutron count across the full energy range for the temperature pair 635° and 735°C. The change in transmission values are as expected much reduced, as the temperature range has been decreased by a factor of approximately seven, but the temperature effect is still present. Analysis for the whole set of resonances yields ΔT ~ 5.1°C - only slightly lower than the apparent accuracy at lower temperatures.

Data from all the runs made show as expected that :

(a) ΔT increases slowly with increasing temperature,

(b) The presence of the hafnium resonances in particular enhances the information content of the exposures and results in the lowest values for ΔT in the Rolls Royce material,

(c) The thicker tantalum foil (106 μm) gives substantially better accuracy than the thinner foil (26 μm).

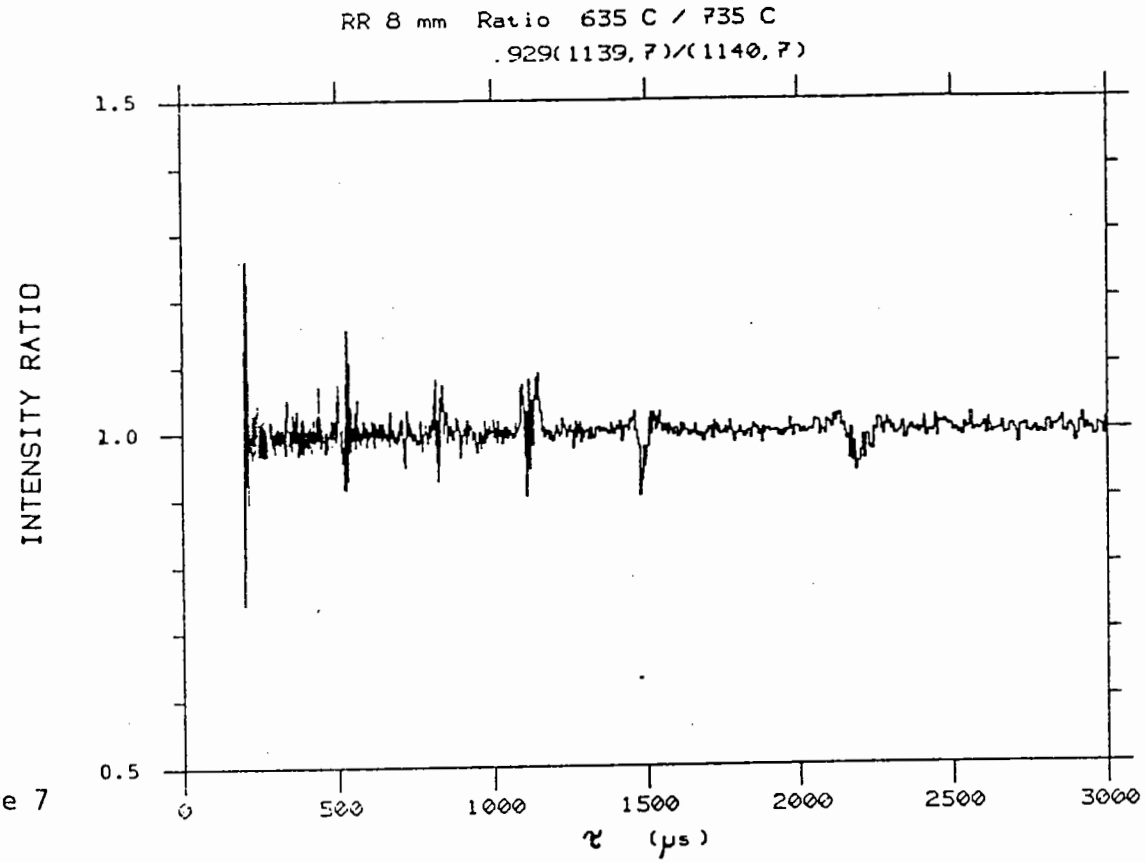

Figure 7

The intensity ratio across the full energy range for the temperature pair 635°C and 735°C.

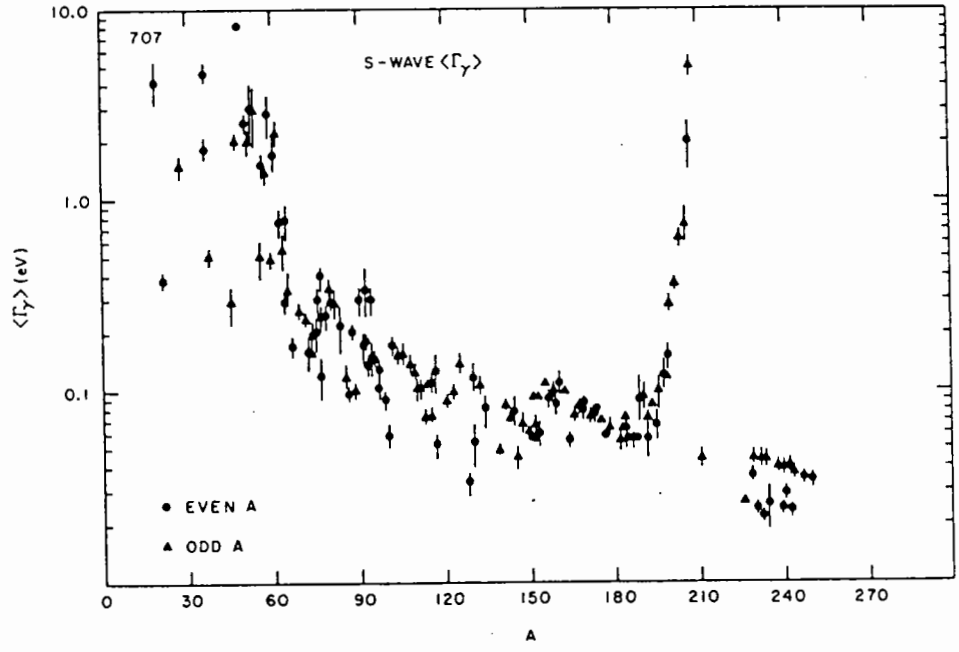

Figure 8

The above shows the width Γ_γ due to the emission of γ-rays following neutron capture, as a function of atomic weight of the nuclei. The full width Γ equals $\Gamma_\gamma + g\Gamma_n$. The quantity $g\Gamma_n$ varies widely from resonance to resonance but is usually less than Γ_γ.

A fuller tabulation of the results from the pair of runs at 22°C and 735°C is given in Table 2, where the signal from the 25 principal resonances is presented, and compared to the accuracy expected according to the theory. Allowance is made for the effects of neighbouring broad resonances that reduce the neutron flux at nearby energies especially the 18.84 eV W^{186} resonance and the 132 eV Co^{59} resonance. The effect of the cadmium resonance at 27.5 eV is also taken into account. The experimental accuracy overall is ~ 25% less than theory prediction corresponding to a loss of ~ 40% of temperature information; this occurs progressively at the high energies. We feel this is due in the main to insufficient timing resolution, the pulse being ~ 4 μs in width. At ISIS in our newer runs we experience the same effect, with the smaller proton pulse width of ~ 0.5 μs largely being negated by the used of smaller beam lengths - ~ 12m as compared to ~ 32m used at Los Alamos. There is however a small discrepancy even for the low energy hafnium resonances where the time resolution is clearly sufficient, which may in fact be caused by background neutrons.

The temperature measurements described above are in detail the mean temperature of the atoms of the particular nuclide that forms the resonance, the mean being taken over the neutron path, If, say, tantalum is present in a blade - and not in any other material in the beam - the temperature from the tantalum resonances applies to the blade only. Further, if for a special purpose, we were allowed to coat several particular surfaces we could get several temperature measurements, including perhaps the most critical temperature, from the same exposure for each pixel. Such a case might occur, for example, for a static blade in an engine where one could use for the front surface Hf, for the inside of the air vents Re, and the rear Pt; with the blade itself containing W and Ta one could form a potentially most informative picture of the temperature distribution.

In practice these measurements will not easily give one an absolute temperature measure, rather they are like a mercury in glass thermometer which one should calibrate at two preferably well-spaced temperatures. Thus the accuracies quoted refer to that which one could obtain in the comparison of two temperatures, one of which is known. One can have faith that the scale is a steadily increasing function of temperature, appropriate for reliable interpolation.

TABLE 2

Eo eV	τ μs	Isotope	Γ meV	$2g\Gamma_n$ meV	Δ_{290} meV	σ_o barns	I	ΔT^{obs} °K	ΔT^{exp} °K
1.098	2194	Hf 177	68	1.92	18	6270	4100	11.1	10.4
2.38	1489	Hf 177	70	8.8	26	13100	4730	10.4	8.6
4.16 }	1127	W 182	51.5	2.94	34	4460 }			
4.28 }	1111	Ta 181	57	4.4	34	23450 }	7420	8.3	6.8
5.68)	964	Hf 179	64	4.2	40	1920)			
5.89)	947	Hf 177	70	5.1	41	3020)	1410	19.0	15
6.60)	894	Hf 177	75	11	43	5350)			
7.65 }	831	W 183	72	2.6	44	903 }	2450	14.2	10
7.78 }	824	Hf 178	110	100	46	42000 }			
8.88	771	Hf 177	72	6.8	50	2600	194	51	40
10.34	714	Ta 181	60	4.1	53	8070	1240	20	15
13.95	615	Ta 181	53	1.14	62	2004	67	87	56
18.84	529	W 186	337	574	76	34100	26	140	78
21.2	498	W 182	101	78	76	12600	1120	21	16
23.9	469	Ta 181	60	6.5	81	5900	31	130	32
27.05	441	W 183	119	63	86	3690	453	33	21
35.16)	387	Ta 181	76	9.3	99	4520)			
35.90)	383	Ta 181	80	16.9	100	7650)	186	52	22
39.13	367	Ta 181	100	44.8	104	14900	404	35	20
46.24)	337	W 183	209	210	112	4100)	429	34	20
47.8)	332	W 183	193	58	114	1170)			
99.32 }	230	Ta 181	165	115	166	9250 }	22	150	50
101.1 }	228	W 183	145	120	166	1540 }			
132	199	Co 59	5530	5770	348	10600	--		
337	124	Mn 55	22900	18700	575	3270	--		
							Σ24,282 ->	4.6	3.6

Details of all the prominent resonances are given for the two runs at 22°C and 735°C. The sensitivity to temperature change for each resonance is indicated by the information I, and the corresponding error in temperature estimate is given enabling immediate comparison of the effectiveness of the various resonances. Most of the information is provided by the lower energy resonances, with the doublet from W 182 and Ta 181 at ~ 4.2 eV being the most informative.

Also given is the theoretical accuracy obtainable for each resonance with the exposures involved. The values of I that are given are the sums carried over each resonance or group of resonances of the quantity ΔI,

$$\Delta I = \frac{[\mathrm{Ln}(N1/N2) - \mathrm{Ln}(N_1^{\,0}/N_2^{\,0})]^2}{1/N_1 + 1/N_2} - 1$$

With N_1 and N_2 the observed neutron counts at the same drift times in the two runs, and $N_1^{\,0}/N_2^{\,0}$ the ratio of the neutron exposures for the runs.

The resonances that are most sensitive to Doppler broadening are those that are intrinsically narrow, but at the same time strong so that not much of the element is necessary to give substantial attenuation at the resonance centre. Figure 8 shows a scatter plot of the γ-ray width versus isotope. This width dominates the full width Γ for all low energy resonances. The sharpest resonances are found in a restricted set of nuclei especially for elements $70 < Z < 76$ $(175 \leq A \leq 190)$, and $Z \geq 90$ where both thorium and uranium possess very narrow resonances., Many but not all of these nuclei have suitable strong resonances Tables 3 and 4 give details of the most prominent and informative resonances of refractory elements and those that are volatile or have volatile compounds. The refractory elements are candidates for thin plated coats or inserts. Also given is the optimum thickness for maximum information from the resonances listed. This is a broad optimum, as a factor of four less or more only reduces the information by a factor of 2.

In these Tables the temperature considered for measurement is 870°K, and the value of I for each resonance is a measure of the temperature information it should yield theoretically with statistical errors that will accompany the exposure to a beam of intensity at energy E in eV :

$$dN_n = 1.0 \times 10^7 \, dE/E^{0.8} \qquad \text{neutrons}$$

with a detector efficiency ε corresponding to 1 cm thickness of Li^6 loaded glass scintillator

$$\varepsilon = 1 - \exp - \sqrt{\frac{3.2}{E}} \qquad \text{with E in eV.}$$

TABLE 3

Element			E_o	$2g\Gamma_n$	Γ	σ_o	Δ	Z	Optimum thickness	Optimum		100 μm	
		%	eV	meV	meV	barns	meV		mg/cm^2	I_1	ΔT_1 °K	I_2	ΔT_2 °K
Mo	95	15.7	44.70	200	316	3,000	265	0.84	1,600	96	10.2	15	26
Rh	103	100	1.26	0.77	156	5,100	43	0.28	340	114	9.4	100	10.0
Ag	109	48.2	5.19	19.10	149	15,800	85	0.57	190	220	6.7	183	7.4
Sm	149	13.8	0.87	0.89	61	3,100	31	0.51	1,200	384		29	
	147	15.0	18.30	79	168	5,100	137	0.82		141		10	
										525	4.4	39	16
Tm	169	100	3.90	12.20	116	35,600	59	0.51	120	167	7.7	167	7.7
Lu	175	97.4	5.95	1.50	62	5,900	67	1.08	880	350		45	
			11.00	3.10	44	8,100	98	2.23		300		26	
			13.80	20	95	19,600	109	1.15		250		94	
										900	3.3	165	7.8
Hf	177	18.5	1.10	1.92	68	6,300	31	0.45	560	260		130	
	177	18.5	2.38	8.80	69	13,100	45	0.65		340		210	
	178	27.2	7.78	100	120	38.400	81	0.68		80		173	
										600	3.8	513	4.4
Ta	181	99.8	4.28	4.40	57	23,800	59	1.03	600	480		325	
			10.34	4.10	60	8,700	92	1.53		240		75	
			35.90	16.90	80	7,800	171	2.14		92		22	
			39.10	44.80	100	15,100	180	1.80		147		49	
										959	3.2	471	4.6
W	182	26.3	4.16	2.94	51	4,750	59	1.16	2,600	590	4.1	83	11.0
Re	185	37.5	2.16	3.30	50	13,000	42	0.72	480	405	5.0	290	5.9
Ir	191	37.4	0.65	0.54	73	5,000	22	0.31	950	140		117	
	193	62.6	1.30	0.91	88	6,500	32	0.36		120		120	
	191	37.4	5.36	6.00	97	5,700	64	0.66		200		94	
	191/3	100–	9.07	3.60	88	6,100	63	0.97		220		80	
										680	3.8	411	4.9
Pt	195	33.8	11.90	15.20	127	4,500	94	0.74	2,300	140		44	
			19.60	10.40	107	2,200	123	1.15		135		11	
										275	6.0	55	13.5
Au	197	100–	4.91	19.00	139	38,700	61	0.44	120	105	9.7	105	9.7
Th	232	100–	21.30	3.80	25	9,200	119	4.76	1,800	310		9	
			23.40	6.70	28.4	13,300	123	4.32	430			18	
			59.50	8.10	27.2	6,600	198	7.20		190		2	
			69.10	88.00	66	25,400	211	5.20		126		28	
										1056	3.1	55	13.5
U	238	99.3	6.67	3.00	27.5	21,600	64	2.33	1,500	780		170	
			20.90	17.40	34	31,900	114	3.28		520		90	
			36.80	64.00	57	39,800	151	2.04		270		90	
										1570	2.5	250	5.4

Details are presented for the most prominent and informative resonances of refracting element that can assist temperature determination. Columns 2–5 give details of the resonances together with σ_o for the element itself; this cross section applies at the resonance energy in the absence of temperature broadening. Columns 6 and 7 give the value of Δ the temperature broadening, and the ratio $Z = \Delta/\Gamma$ which in conjunction with σ_o is decisive in determining the information content of the resonances for a given quantity of the material in the beam. The optimum thickness, given in column 8 for each element is that which maximises the total information content from the resonances included. Columns 9 and 10 give the values of the information content T_1 for each resonance when using the optimum thickness, and ΔT_1 the accuracy attainable from over the resonances. Likewise in columns 11 and 12 a layer of the element of 100 μm thickness is assumed. Usually this is considerably below the optimum, and the accuracy suffers accordingly.

TABLE 4

Element	%	E_o eV	$2g\Gamma_n$ meV	Γ meV	σ_o barns	Δ meV	Z	$3.10^{19}/cm^2$ I_1	ΔT_1 °K	$10^{20}/cm^2$ I_2	ΔT_2 °K	Remarks: volatile component
In 115	95.7	1.46	3.34	75	38,000	43	0.57	58	13	230	6.6	$In(CH_3)_3$
Xe 131	21.2	14.40	270.00	309	17,020	128	0.41	3.2	36	19	23	Gas
Cs 133	100.0	5.90	5.40	120	10,100	81	0.68	2.8	110	19.2	23	
Sm 152	26.7	8.05	260.00	196	58,200	88	0.45	29	18	71	12	$SmCl_3$
Hf 178	27.2	7.73	100.00	120	41,730	81	0.68	18	23	80	11	$Hf(CH_3)_4$
W 186	28.6	18.84	574.00	337	34,100	123	0.365	6	41	21	22	WF_6

Columns 1–5 give data for the resonances of the isotopes of chemical elements that have both a volatile compound and a suitable strong resonance. Column 6 gives the cross section for the element at the resonance energy in the absence of thermal broadening. In columns 7 and 8, Δ represents the broadening and the Z the ratio Δ/Γ that together with the value of σ_o is decisive in determining I, the information content of the resonance for the amount of material in the beam. Values for 3×10^{19} and 10^{20} atoms/cm^2 of the seed material are given in columns 9–12, together with the corresponding figures for the accuracy of the determination of the gas temperature, ΔT.

For these figures a neutron exposure of $10^8\ dE/E^{0.2}$, and a representative value of 870°K have been taken.

NEW MEASUREMENTS

Recently we have repeated these early measurements at ISIS in the UK [2] with a small glass scintillation detector which is a prototype for a high count rate multi-pixel array of detectors, each individual pixel of which should be able to yield its independent temperature estimates for each resonance. Two examples of these recent measurements are given in Figure 9. For the first a tantalum foil of thickness 500 μm was employed. This thickness is sufficient to allow considerable temperature sensitivity for the higher energy resonances as well as the very strong 4.28 eV resonance. The detector presented an area of 1 mm^2 to the beam, and had a thickness of 1 cm. The accompanying Table gives details of the temperature information achieved from each resonance from the data, and that expected from the exposure using the resonance data for tantalum and the known foil thickness. The agreement is satisfactory, though analysis is continuing to evaluate the contributions due to background and other effects.

TABLE 5

500 μm Tantalum Foil

20°C and 182°C

Eo eV	Drift Time μ sec	Experimental Information Y′ (ΔT = 162°C)	± ΔT °K	Theory ± ΔT °K
4.28	423.5	2540	3.2	4.2
10.34	272.1	2670	3.1	3.6
13.95	234.1	410	8.0	6.1
23.90	178.6	890	5.4	5.2
35.16	147.1	1740	3.9	4.3
35.90	145.6			
39.13	139.4	480	7.4	5.7
99.32	87.1	100	16.2	12.8
		Σ = 8830 →	± 1.7 →	± 1.85

Table 5 displays the information for tantalum exposures at two values of temperature. In each run the spectrum of detected neutrons was about 1.0×10^5/μs. A single detector or area $1(mm)^2$ only was used as a test for a prototype multipixel array. As in Table 2 it is clear that experimental information is less readily obtained at high energies.

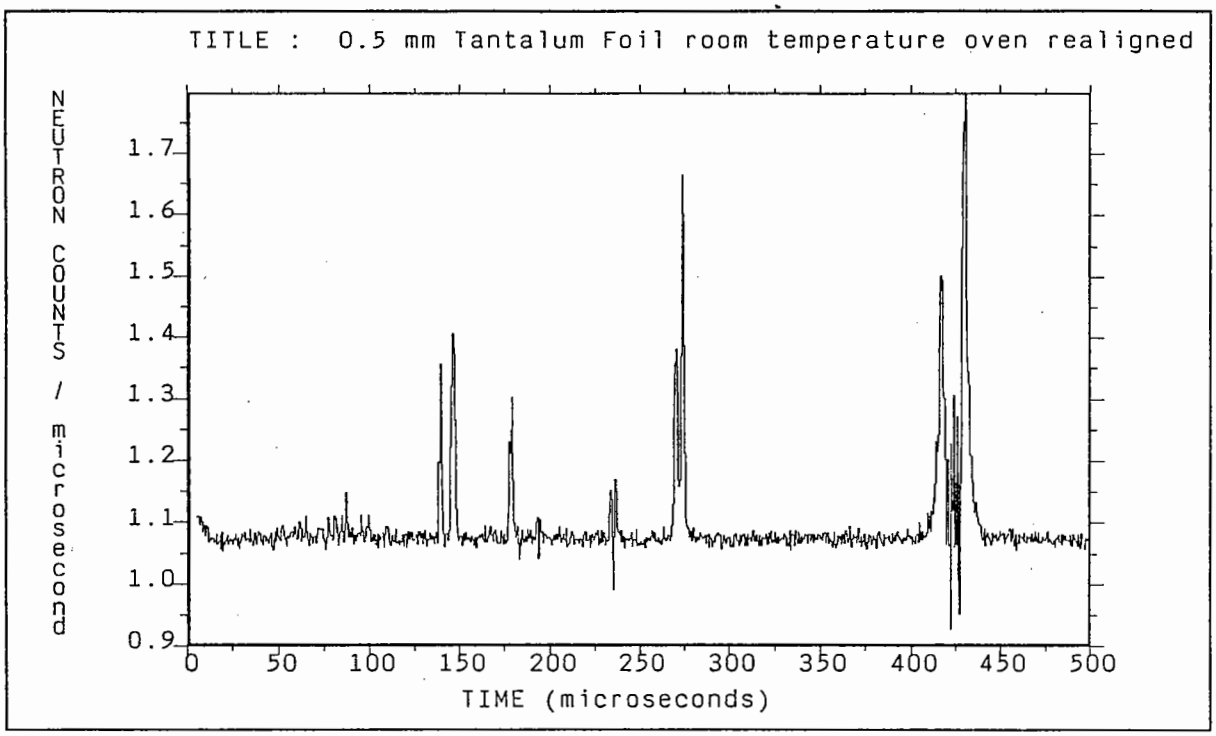

Figure 9

Recent data taken at ISIS for the ratio of the neutron counts between two exposures of a 0.5 mm tantalum foil at 20°C and 182°C. The effect of temperature on the transmission is clear and detailed analysis is proceeding.

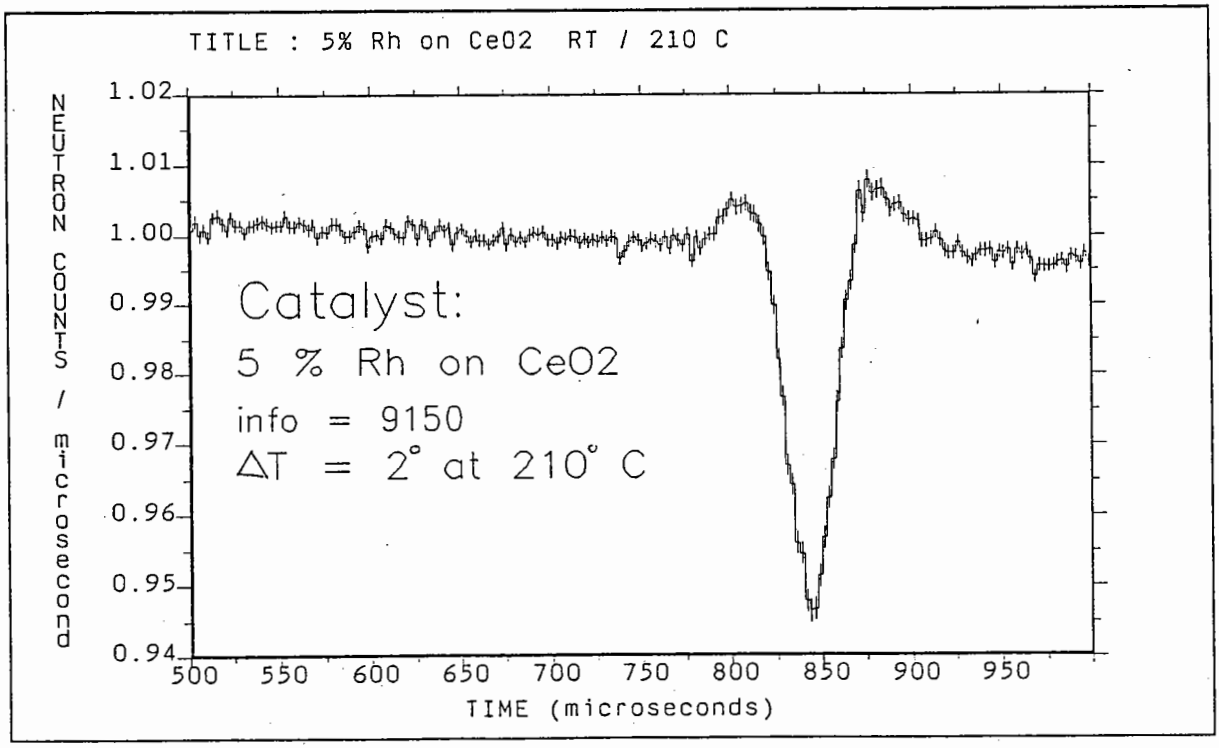

Figure 10

The ratio of neutron counts between two exposures of a catalytic material at 20°C and 210°C. The active element is 5% rhodium on a CeO_2 support. This test was recently performed at ISIS.

The second series of measurements involved some sample catalyst materials such as 5% Rhodium om various oxides. Rhodium possesses one useful resonance at low energy. Figure 10 displays the ratio of counts between 20°C and 210°C for a long exposure which indicates that one can use good statistics to obtain a considerable response from a modest temperature change. Analysis of these data showed an estimated accuracy of $\Delta T = +/- 2^{o}C$.

FUTURE POSSIBILITIES

At Los Alamos each time of flight spectrum took us about 8 hours to accumulate, a feature which has been remedied with higher neutron flux and an improved detector. During the early commissioning phase ISIS will give us more neutrons than were available at Los Alamos in 1984 (considerable enhancement has also taken place there in the intervening period), and that will increase by a further factor approaching 10. ISIS at the Rutherford Appleton Laboratory can provide us not only with adequate neutron fluxes, but also with an ideal environment for the development of the technique so as to prove (or otherwise!) its practicability.

BEAM PROPERTIES AND FLUXES AT ISIS

To make the best use of transmission experiments operating in the direct neutron beam at ISIS details of the properties of the beams must be understood. The maximum neutron output from the moderators with the exit jaws wide open is expected to be

$$dN_n \sim 1.0 \times 10^{13} \frac{dE}{E} \text{ neutrons/steradian sec,}$$

where E is the neutron energy. The accelerator will operate at 50 pulses per second, and the RMS spread of the proton pulse is ~ 0.25 μs. Each cm^2 of detector at a distance of d-metres, will intercept a flux of neutrons with a time spectrum by :

$$dN_{dnt} \sim \frac{4.0 \times 10^7}{d^2} \cdot \frac{d\tau}{\tau} \text{ neutrons/cm}^2 \text{ pulse}$$

where τ is the travel time of the neutron over the flight path d, τ is given by the relation

$$\tau = d/v \simeq \frac{72.2d}{\sqrt{E_{eV}}} \text{ μs,}$$

when the neutron energy E is measured in electron volts.

The efficiency of the detector for absorbing neutrons must be known before one can establish the magnitude of any problem with count rate due to pile up.

All the epithermal neutron detectors are based on capture, for which the cross section $\sigma \propto 1/V$. So the detector efficiency ε is given by

$$\varepsilon = 1 - \exp\{- E_o/E\}^{1/2} .$$

E_o is a characteristic energy and it naturally depends upon detector thickness and its constitution, and is in fact proportional to the square of the thickness.

TABLE 6

Detector	E_o	τ_o
~ 7 mm He^3 at 10 atm	0.026 eV	448 μs
1 cm Li^6 glass, (5% Li)	3.2	40
1 cm Li^6I	7.1	27

In the brief table above the first entry corresponds to the detectors we employed at Los Alamos, and the remainder are representative of the materials being considered for future high count rate detectors. τ_o is the flight time of a neutron of energy E_o over a path of 1 metre. We therefore can write for the time spectrum of the absorbed neutrons i each pulse as

$$\frac{dN_{Ads}}{d\tau} = \frac{4.0 \times 10^7}{\tau\, d^2} \left[1 - \exp - \tau/\tau_o d\right] \quad \text{neutrons}/\mu s.cm^2$$

At short times, corresponding to high neutron energies, the detection rate tends to a maximum dependent of τ

$$\frac{dN_{Ads}}{d\tau} \rightarrow \frac{4.0 \times 10^7}{\tau_o\, d^3} \qquad \text{neutrons}/\mu s.cm^2$$

Setting d = 20m as representative of time of flight beam lines and τ_o = 40 μs, corresponding to the use of 1 cm of Li^6 glass scintillator, we have

$$\frac{dN_{Ads}}{d\tau} = \frac{1.0 \times 10^5}{\tau} \left[1 - \exp - \tau/800\right] \quad \text{neutrons}/\mu s.cm^2$$

The most relevant band of neutron energy for these temperature measurements is $1' \leq E \leq 100$ eVm and at 20m these limits correspond to $144 \leq \tau \leq 1444$ μs. substituting for these we obtain

$$58 \leq \frac{dN_{Ads}}{d\tau} \leq 114 \qquad \text{detected neutrons}/\mu s.cm^2$$

Note that the rate is high, at $100/\mu s.cm^2$, and that the rate does not change greatly through the pulse. The total number of neutrons detected in this energy band is therefore ~ $10^5/cm^2$ pulse.

PROPOSED DETECTORS

The natural way out of the difficulty posed by the high neutron flux is to have small individual detectors - of 1 $mm,^2$ say - so that the event rate in each element is only ~ 1 per μs - a rate that is readily accommodated. Small detectors will at the same time given one good positional accuracy, and that is clearly beneficial.

These individual detectors - or pixels - must be individually connected to photomultipliers - on a one-to-one basis - to preserve the high count rate ability. A practical device might then contain from 10^2-10^3 pixels. Initially this implies a rather large and even embarrassing number of photomultipliers. However to meet the needs of just such arrays of detectors, multi-anode photomultipliers are being developed in France and in Japan, in which separate areas of the photocathode contribute to just one anode. Such devices are in reality like a large number of tubes within a single moderately sized glass envelope. The number of anodes envisaged per device is ~ 64 in a square matrix.

We therefore propose that an initial high count rate multipixel detector for epithermal neutrons might be built along the lines sketched in Figure 11. It would be modular in form and so one could add to it as desired. The main features are :

1 The detectors would be ~ 1 mm x 1 mm x 10 mm Li^6 loaded scintillating glass.

2 Monofilament fibres would transport the scintillation to an array of photomultipliers.

3 B^{10} shielding would be employed between the scintillators to reduce the response to scattered neutrons to a low level. This will only form a significant background at the higher energies, and when the detector array is large.

Particular care must be taken in the coupling between the scintillator and the fibre so that an adequate fraction of the light is within the NA of the

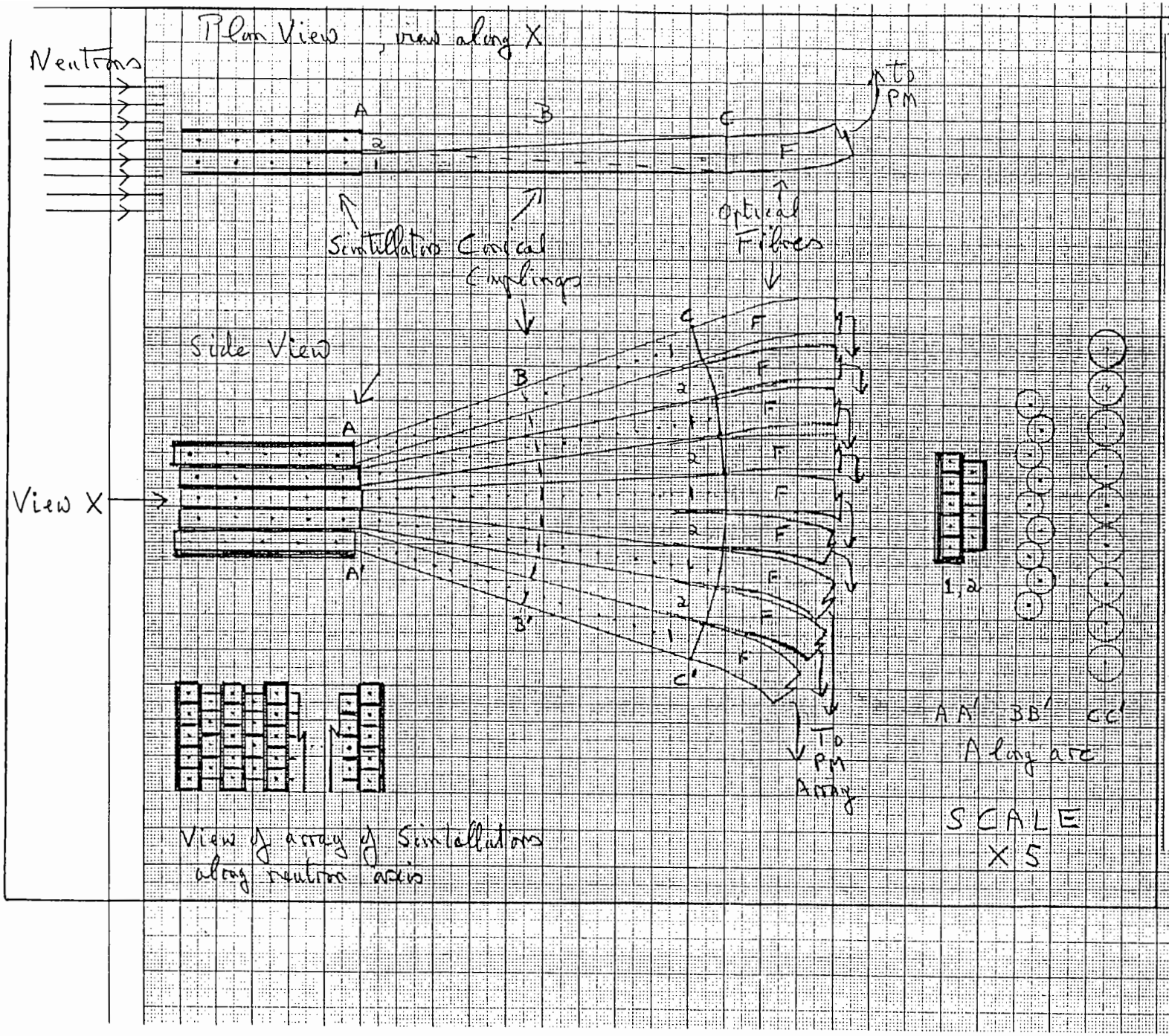

Figure 11

Sketch of possible configuration of high count rate multi-pixel neutron detector.

The detector is modular in form, as drawn a set of 9 pixels comprises the repeat structure which is contained within a width of 2.4mms, as is displayed in the plan view, which illustrates a single module only.

The conical optical coupling devices give an expansion of x 2.0 in diameter, and so increases the NA correctly coupled to the fibre by a similar figure. Larger expansion ratios are possible, but require a greater length for the couplings to avoid undue angular fan-out in the side projection.

monofilament. Additionally one wants a uniform output versus position within the detector of the neutron absorption.

When such a device works to one's full satisfaction, and when suitable multi-anode photomultipliers become available, one can envisage further detector development in two principal directions

1 To cover larger areas ~ with the same pixel size, up to say, 10^4 pixels.

2 To develop a small detector with still higher spatial resolution - pixel size ~ 0.10 $(mm)^2$.

Both these developments may require high numerical aperture imaging optics to match the output of the scintillator to the NA of the fibres that distribute the light to the arrays of photomultipliers.

Alternatively one may wish to leave scintillators and transfer to solid state detectors so as to most conveniently obtain such a large number of closely packed fairly small pixels.

DATA ANALYSIS

The acceptance of the data stream from a detector with less than say 100 pixels, such as envisaged for the initial stage, that yields $\leq 10^8$ neutrons per second is well within the capabilities of the VAX basal system at the RAL, and so it should not present any particularly significant problem.

The data for a run such as is envisaged for each pixel amounts to a histogram for some 2000 essentially independent neutron energies - or time bins. The histogram would contain ~ 10^7 neutrons for each pixel, and would in principle and in practice contain enough information for one to make an independent estimate of the temperature to ~ $\pm$ 5°K for each pixel. Hence a good idea of the temperature field should be obtained with a detail that is much finer than that provided by thermocouples.

MOVING TARGETS

The majority of potential targets for the use of this technique are moving ones. It is much more difficult to obtain data conventionally from moving than stationary parts - especially this is true for instruments having an electrical read out, e.g. thermocouples - where slip rings are necessary. Movement, however, presents no problems to the neutron detector system itself but it does affect data analysis. There are two distinct effects on the data from the measurement of a rotating target, and they must both be removed; they are :

(a) Motion along the line of sight, which moves the resonances bodily. This can readily be removed as the centre of the resonance is easily identified giving an accurate estimate of the relative velocity.

(b) Transverse motion which moves every particular element of the target across the field of pixels. The analysis must be made on an element of the target which must be followed across the field of view and binned accordingly. The motion is very considerable.

If we are considering a target such as a turbine blade, transverse motion of ~ 400 m/sec must be countenanced. This moves across the field in a time of 25 μs/cm. So for a small detector ~ 1 cm in dimension, one cannot necessarily follow one element of the target for a period as large as the span of time on a resonance, ΔT, for which useful information is obtainable. This is particularly the case for lower energy resonances . Table 7 lists a number of the strong resonances from Hf, Ta and W that are the most informative for temperature determination. ΔT shown in column 4 displays the decrease from ~ 200 μs to ~ 1 μs over the range of energy 1-100 eV, when taking a value of 20 m for the neutron flight path.

The movement across the field of view naturally enhances the potential usefulness of the larger detector - and suggests that somewhat elongated arrangements of pixels may be preferable. It also enhances the value of resonances at the higher energies, and on arrangements with shorter values of d - the neutron flight path.

TABLE 7

Resonance	E_o eV	ΔE eV	τ_{20m} μ sec	$\Delta\tau$ μ sec
Hf 177	1.098	0.31	1380	195
Hf 177	2.38	0.37	935	73
W 182	4.16	0.35	708	30)
Ta 181	4.28	0.38	697	31)
Hf 178	7.78	0.60	517	20
Ta 181	10.34	0.50	448	11
W 183	27.05	0.87	277	4.5
Ta 181	39.13	0.93	230	2.7
Ta 181	99.32	1.50	144	1.1

The table gives details of useful resonances obtained in an exposure of MARM002 - a high temperature alloy that contains 10% W, 2.5% Ta and 1.2% Hf by weight.

The spread in energy, ΔE, over which the resonance provides useful data for temperature determination is given, together with the drift time τ and the spread in time ΔT resulting from ΔE. A drift path of 20m has been taken as representative.

Note that the value of ΔT increases quite rapidly with increasing energy, so that high energy resonances are covered in periods that are short compared to the period during which a given element in the moving target is covered by the detector.

The motion of the target across the field can be determined empirically from the pattern of neutron fluxes. Any edges or implants will modulate the neutron intensity sufficiently for them to be positioned in the field of an accuracy considerably better than 1 pixel in dimension. The phase, angular speed and centre of rotation can therefore be determined from the measurements alone, although obviously use would be made of measurements off inductive pick up from the shaft.

If, in fact, there were no significant gradients in the target so that one was not able to look on to its motion, in fact one would not need to follow the element of the target across the field of view, and one could analyse the data, as though it had no such transverse moment, and had line of sight velocity alone.

CYCLIC TEMPERATURE VARIATIONS AND TRANSIENTS

In this area we believe the technique can have a very useful performance. Thermal fatigue can be introduced by either cyclic variations of quasi periodic transients.

(a) Cyclic Temperature Variations

Let us assume a sinosoidal dependence with time imposed on the surface

$$\Delta T = \Delta T_o \text{ Cos } \omega\tau,$$

then the temperature at a depth x in a homogenenous medium as a function of time is given by

$$\Delta T = \Delta T_o \text{ (exp - kx) cos } (\omega\tau - kx)$$

where

$$k = [\omega/2D]^{1/2} \text{ cm}^{-1},$$

and D is the thermal diffusivity which is defined as

$$D = k/\rho c,$$

where k is the thermal conductivity (Cal/sec.°K.cm^{-1})

ρ is the density (g cm^{-3})

and C is the specific heat, (Cal/g)

Taking ω as 10^5 radians per second, and D = 0.25 as being representative, we have for a typical penetration depth (k^{-1}) a value of 22 μm - a significant penetration. The temperature wave thus penetrates sufficiently to get very reasonable absorption in a number of suitable coatings. Such a value for ω is that which is imposed on a turbine blade as it rotates in the gas flow behind nozzle guide vanes.

Table 8 gives details of some possible coatings that could be employed, including penetration depths for the thermal wave and the neutron mean free paths for the best resonances. The material chosen for the coating MUST be one that is absent in the bulk material so that the temperature measured applies to the coating alone. For all these materials the temperature wave penetrates to depths of comparable to or deeper than the neutron mean free path enabling precise measurements of the fluctuating component to be made. Accuracies of ΔT of the order of $\pm$ 5°K appear possible in times of order of 3 minutes exposure at the proposed rate of data acquisition 1 neutron/μs for each pixel.

(b) Temperature Transients

Additional to the high frequency thermal field imposed on turbine blades, there are variations in engine conditions expected during flight due to the use by pilot of his controls. These variations have a large amplitude and it is the general view that these repeated transients are the main limit to the life of parts of engines.

The expected thermal behaviour of the specimen to the supposed step function in the conditions depends naturally - and critically - on the boundary conditions, two extremes of which are :

(a) That the surface experiences a step function in temperature, of magnitude ΔT_o

or

(b) That the environment experiences the step function ΔT_o - so that the heat flow into the surface experiences the jump.

This step so induced propagates steadily into the specimen of thickness 2λ and the mean temperature through the specimen is given approximately by

$$\Delta T_{mean} \simeq \Delta T_o \left[1 - \exp\left(\beta \frac{\pi^2 D}{4\lambda^2} \tau\right)\right] .$$

This is a reasonable fit for all values of τ. In this expression D is the thermal diffusivity and β the numerical factor. Figure 11 displays the full calculated results for the propagation of the temperature step for the

TABLE 8

Element	No. of useful Resonances	Principal Isotope	Resonance Energy eV	λ 290°K μm	Melting Point °C	Density g cm^{-3}	Thermal Diffusivity cm^2/sec	Thermal Penetration ($\omega = 10^5$) μm
42 Mo	1	95	44.7	71	2620	10.2	0.54	33
45 Rh	1	103	1.26	28	1966	12.5	0.49	31
47 Ag	3	109	5.09	14	960	10.5	1.71	58
62 Sm	4	152	8.05	6.2	1077	7.8	0.10	14
69 Tm	2	169	3.90	10.1	1545	9.3	0.11	15
72 Hf	3	178	7.78	7.4	1700	13.3	0.16	18
73 Ta	4	181	4.28	11.2	3000	16.6	0.34	26
74 W	3	182	21.2	20	3410	19.3	0.67	37
75 Re	1	185	2.16	15	3170	20.5	0.17	18
77 Ir	4	191	5.36	31	2450	22.4	0.51	32
78 Pt	2	195	11.9	42	1772	21.4	0.25	22
79 Au	2	197	4.91	5.1	1063	19.3	1.26	50

The elements listed above are suitable for high temperature measurement, and all possess at least one good resonance.

The right hand columns give figures for the metal, Rare earth oxides, e.g. Sm_2O_3 and Tm_2O_3 are suitable candidates for incorporation into Syalon ceramics.

surface, the centre and the mean temperature of the slab as a function of time. Nevertheless the empirical approximation above is useful to get a feeling for the duration of the transient. For condition (a) $\beta = 1.0$, for condition (b) the value of β depends upon the efficiency of the heat transfer from the gas to metal and the thermal conductivity of the metal itself, and is always less than unity. For metal blades β is likely to be in the range $0.05 < \beta < 0.5$. The duration of the transient

$$\tau_o \sim \frac{4\lambda^2}{\pi^2 D\beta} \quad \text{seconds}$$

second, so for small turbine blades with $\lambda \sim 0.3$ cm, $D \sim 0.1$ cm^2/sec, and $\beta = 0.1$ say $\tau_o \sim 4$ sec; τ_o is larger still of course for thicker structures.

Thus the temperature transients in the metals last sufficient time for one to be able to measure their decay with some accuracy, as a function of both position and time - if it is a repeated transient. This is the case of those produced by transitions involved in engine tests. With a single transient one would only be able to collect sufficient data on thicker components. If the component is too thick, however, i.e. ≥ 4 cm of nickel alloy, then the neutron penetration itself becomes insufficient. Here we note that ceramic structures such as those fabricated from β' syalon have quite different thermal properties - and are somewhat more transparent to neutrons so that ~ 7 cm of material can usefully be penetrated.

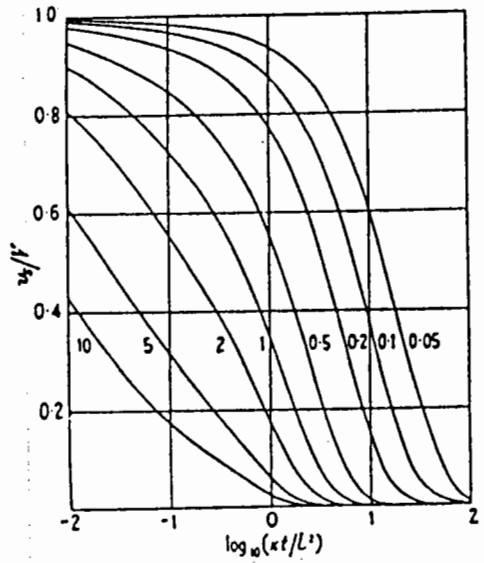

FIG. 17. The function $[1-f_1(L, T)]$ defined in (2). The figure shows the surface temperature v, of a slab of thickness $2l$, initially at temperature V, and cooling by radiation into a medium at zero. The numbers on the curves are values of $L = lh$.

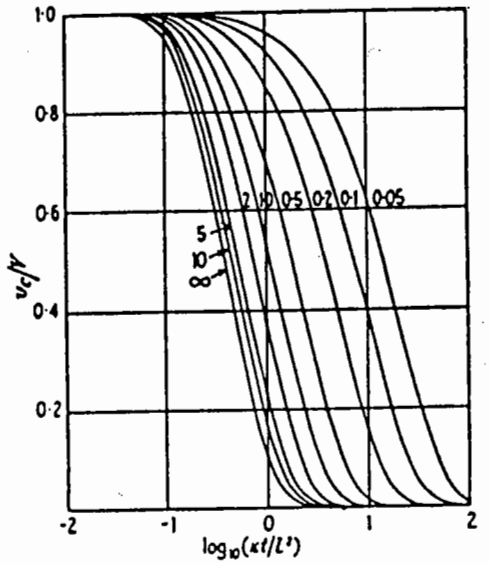

FIG. 18. The function $[1-f_3(L, T)]$ defined in (3). The figure shows the centre temperature of a slab of thickness $2l$, initially at temperature V, and cooling by radiation into a medium at zero. The numbers on the curves are values of $L = lh$.

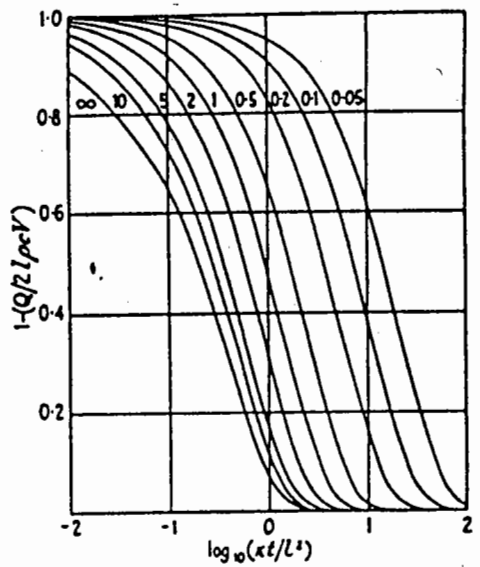

FIG. 19. The function $[1-f_5(L, T)]$ defined in (4). The figure shows the heat Q lost from unit area of a slab of thickness $2l$, initially at temperature V, and cooling by radiation into a medium at zero. The numbers on the curves are values of $L = lh$.

Figure 12

These plots are taken from "Conduction of Heat in Solids" by Carslaw and Jaeger. They show the fraction $\Delta T/\Delta T_o$ for the surface, the centre and the mean temperature through the slab for the transient. The curves are labelled with the appropriate value of L. $L = \infty$ corresponds to the situation where the surface temperature immediately jumps to the new equilibrium value. The number L is given by $L = \ell H/K$, where H is the heat flow into the solid per (unit area.^oK.sec), and K is its thermal conductivity.

The x coordinate, plotted with a logarithmic scale, is $D\tau/\ell^2$, and the y coordinate v/V is the complement of that given opposite and is $(1 - \Delta T/\Delta T_o)$, so that it tends to zero not unity as $\tau \to \infty$.

SUMMARY OF THE POSSIBILITIES OF TEMPERATURE MEASUREMENT WITH EPITHERMAL NEUTRONS

Utilisation of high count-rate neutron detectors with a small pixel size on time of flight beam lines gives one the capability to measure the temperature field with a precision $< \pm 5°K$ at all temperatures $\leq 1000°K$ in a reasonable time. Each pixel will yield an estimate of temperature independent of its neighbours, and one can consider in the future arrays of up to say 10^4 pixels. With the use of thin coatings of suitable materials not present in the bulk specimen, e.g. Re Ir, Au, etc, one can simultaneously measure the temperature field at several depths insofar as the resonances do not overlap.

Measurement of the temperature field gives one much more data that is usually obtained from a small number of sensors - and so will lead to a greater understanding of the temperature field.

One can also measure temperature transients with comparable accuracy to that of the mean temperature and determine its development with time and as a function of position. This is best done if the transient is repeated a number of times, so that data can be accumulated for a number of nominally identical transitions.

The paragraphs above apply to stationary targets. Moving specimens can also be measured, and temperatures determined with comparable accuracy in temperature determination. But one has to live with the fact that the specimen may be in the field of view for a small fraction of the time - except with large arrays of detectors.

The usefulness of such measurements appears to have immediate applications for the Aero-Engine Industry, where turbine blades provide an obvious target whose life and performance is limited by thermal effects - both static and cyclic - through thermal fatigue. It is also of significance that one measures the true metal temperatures below any thermal barriers that may be used.

Thrust bearings are also an attractive target, their performance is also similarly restricted by thermal effects. For such a target the neutrons can

not only tell us the temperature of the rollers or balls, and their housings, but also can enable one to evaluate the rotation axis of the balls and their angular velocity and bulk motion, so determining the position and degree of slip. This could clearly be done as a function of the operating conditions of the bearing.

Attractive applications appear possible for car engines. Here one may have to deal with reciprocating rather than rotating components, but spiritually this is the same.

Recently interest has been shown in the possibility of measuring various catalysts while they are in operation, to determine where possible the surface temperatures.

REFERENCES

[1] P H Fowler, A D Taylor and P A Seeger, 'Neutron Resonance Radiography as a Non Invasive Temperature Probe' (in preparation).

[2] P H Fowler, A Gay, R Head, A D Taylor, Z A Bowden and R C Ward, unpublished data.